Journal of Archaeological Science 155 (2023) 105777

Contents lists available at ScienceDirect

Journal of Archaeological Science

journal homepage: www.elsevier.com/locate/jas

Accelerating the discovery of new Nasca geoglyphs using deep learning

Masato Sakai [a,*,1], Yiru Lai [b,**,1], Jorge Olano Canales [c], Masao Hayashi [b,1], Kohhei Nomura [b]

[a] Faculty of Literature and Social Sciences, Yamagata University, Yamagata-shi, Yamagata, 990-8560, Japan
[b] Technology, IBM Japan, Ltd., Chuo-ku, Tokyo, 103-8510, Japan
[c] Archéologie des Amériques, Université Paris 1 Panthéon-Sorbonne, Paris, 75004, France

ARTICLE INFO

Keywords:
Nasca
Geoglyph
High-resolution aerial photograph
Remote sensing
Deep learning
Object detection

ABSTRACT

We discuss an archaeological research of employing deep learning (DL) based object detection on high-resolution aerial photographs to discover Nasca geoglyphs, which have been designated as a UNESCO World Heritage Site. Owing to extremely limited archaeological ground truth data and their differences in scale and design, it is difficult to detect new geoglyphs merely training DL on the known geoglyphs. Therefore, we developed a pipeline of DL to mine such data and address the challenges unique to archaeology. With this approach, we identified four new geoglyphs in the northern area of the Nasca Pampa, namely: a humanoid, a pair of legs, a fish, and a bird. The geoglyphs got verified through on-site surveys. We could identify new geoglyph's candidates approximately 21 times faster than with the naked eye alone. The approach would be beneficial for the future of archaeology in a new paradigm of combining field survey and AI.

1. Introduction

Archaeology is a discipline studying the past. However, the archaeological community has also thrived to adapt the most cutting-edge science and technologies. Recent advances in automated sensing enabled by the proliferation of drones, robotics and Light Detection and Ranging (LiDAR), Big Data, and artificial intelligence may fuel the next wave of archaeological discovery. For example, these technologies are used for the detection and analysis of difficult-to-reach terrestrial or marine archaeological sites, or for the analysis of the shape and iconography of fragments, documents, and inscriptions found during archaeological excavations (Mantovan and Nanni, 2020; Pecci, 2020). Yamagata University led a large-scale project to test-drive these technologies with the aim of identifying gaps and learning lessons and best practices for future projects of similar nature. A feasibility study using DL was part of the project.

1.1. Discovery of Nasca geoglyphs

The geoglyphs were discovered at the Nasca Pampa starting in the 1920s with lineal one (Mejía Xesspe, 1942; Kroeber and Collier, 1998). Later in the 1940s, various figurative geoglyphs, including hummingbirds, monkeys, flowers, and tools were discovered (Reiche, 1993). In the 1980s, interdisciplinary field research was conducted on geoglyphs using photographs taken from air balloons and airplanes maneuvering over the Nasca Pampa (Aveni, 1990).

The purpose of making geoglyphs was discussed in relation to the astronomical event (Kosok, 1965; Reiche, 1993). However, this theory is not necessarily accepted today. Rather, it is more likely that they were produced for ceremonial walking (Aveni, 1990; Lambers, 2006, 2020; Mejía Xesspe, 1942), while the presence of pottery fragments (Clarkson, 1990), maize and spondylus (Reindel et al., 2006) found on geoglyphs suggests that they were the site of ceremonial activity.

In 1993, the Nasca geoglyphs were registered as a UNESCO World Cultural Heritage Site, and subsequently, preservation plans were developed by the Peruvian government (Lumbreras, L. G., 2000). However, in those days, there was limited effort to record the distribution of geoglyphs in the Nasca Pampa. As a result, illegal development activities frequently led to the destruction of geoglyphs posing a social problem (Specia, 2018). Thus, it is critical to understand the distribution of Nasca geoglyphs to preserve these important archaeological monuments.

Since 2004, Yamagata University has been conducting geoglyph distribution surveys using satellite imagery, aerial photography,

* Corresponding author.
** Corresponding author.
E-mail addresses: sakai@human.kj.yamagata-u.ac.jp (M. Sakai), e35553@jp.ibm.com (Y. Lai).
[1] These authors contributed equally to this work.

https://doi.org/10.1016/j.jas.2023.105777
Received 5 December 2022; Received in revised form 2 April 2023; Accepted 20 April 2023
Available online 1 June 2023

airborne scanning LiDAR, and drone photography to efficiently investigate the vast area of the Nasca Pampa covering more than 390 km^2 (Sakai et al., 2014, 2019, 2021; Sakai and Olano, 2017).

Geoglyphs can be categorized into three main types: figurative, geometric, and lineal (Aveni, 1990). The figurative ones, which comprise animals, humans, plants, and tools, are further classified into line-type and relief-type according to the method of their creation (Fig. 1). Many line-type geoglyphs were drawn in a single stroke as a white line. In contrast, the relief-type was drawn as a combination of white and black parts of the figurative geoglyphs. Owing to the differences in the combination, the relief-type geoglyphs can be categorized into four subtypes (Fig. 1B–E).

The line-type was argued to have been produced during the Nasca period (A.D.100-650) because of their similarity to the iconography of Nasca pottery (Isbell, 1978). The relief-type, on the other hand, is believed to belong to the late Formative period (400-200 B.C.). This is because the iconography of latter type of geoglyph is similar to that of the Formative petroglyphs, and it is thought that the iconography originally on the rock came to be depicted on the geoglyphs as well (Reindel et al., 1999).

In 2016, we acquired aerial photography with a ground resolution of 0.1 m per pixel utilizing an aerial survey digital camera rasterizing the entire area of the Nasca Pampa. In addition, detailed topographic data from airborne LiDAR scans has been acquired. Analysis of these images revealed several small relief-type geoglyphs. Therefore, we conducted a field survey to identify these geoglyphs. Aerial photographs are useful for mapping the distribution of geoglyphs because their resolution is considerably higher than that of the satellite imagery at hand with ground resolution of 0.61 m per pixel.

The Nasca Pampa is very large, and it would take a considerable amount of time for the naked eye to search for geoglyphs in high-resolution images. With such a human effort, our team took about five years to analyze the satellite data. Therefore, we can estimate that more time and effort will be required to analyze the very high resolution (VHR) aerial photographs. To effectively detect the location of new geoglyphs on the aerial photographs, we decided to introduce object detection using DL (Goodfellow et al., 2016) trained with the data of known geoglyphs. The aim is to significantly accelerate the discovery of new geoglyphs using DL.

Northern area of the Nasca Pampa (latitude 14°40′11″–14°42′47″S and longitude 75°5′44″– 75°8′52″W) was chosen as a test area where well-known large animal and plant geoglyphs are concentrated *(2)* (Fig. 2). And we picked figurative line-type geoglyphs as the target of detection. The chosen area amounts for about 9% of the total Nasca Pampa area. Two criteria guided us in selecting this area: (a) there is a high concentration of figurative line-type geoglyphs in the area that provides more training data for DL compared to other areas; (b) the location has been more intensively investigated than other areas of the Nasca Pampa and includes most of famous geoglyphs. Therefore, if new geoglyphs get discovered with the aid of DL in this area, we can successfully demonstrate the value of DL in the discovery of Nasca geoglyphs.

1.2. Deep learning

DL is a particular kind of machine learning that achieves great power and flexibility in pattern analysis of images, speech, language, and more. In archaeology, DL is used in the analysis of the iconography, text, and writing of excavated objects (Barucci et al., 2021, 2022; Clanuwat et al., 2019; Lamb et al., 2020; Roman-Rangel and Marchand-Maillet, 2016). Other areas of DL application is in the remote sensing domain (Zhu et al., 2017). While traditional image processing methodologies require explicit rules for detecting target features, DL is able to learn representations from large amounts of training data. In archaeology, to discover ground structures via LiDAR (Lidar 101, 2012; Albrecht et al., 2019) or aerial photographs studies using DL have been applied for image classification (Caspari and Crespo, 2019; Kazimi et al., 2018; Soroush et al., 2020), object detection (Character et al., 2021; Trier et al., 2021; Vaart and Lambers, 2019), and combinations of object detection and segmentation (Guyot et al., 2021a, 2021b; Bonhage et al., 2021; Davis et al., 2021) tasks. Compared to these studies, our research faces challenges in terms of the small number of training data and the diversity of the design in the object we want to detect.

In 2018, we conducted a proof-of-concept (PoC) study using a "Single Shot MultiBox Detector" (Liu et al., 2016), which is one of the popular object detection algorithms (Liu et al., 2020) adopting the DL paradigm. Object detection is a task to identify and locate objects of certain classes within an image. Our goal was to efficiently find new geoglyph's candidates based on wide-ranging aerial photographs. After the PoC, our on-site survey was conducted until February 2020 to verify the results of our study.

2. Material and methods

2.1. Dataset of aerial photographs

The image dataset employed covers an area of 27 km^2 along the Ingenio Valley in the northwestern part of the Nasca Pampa. To build a DL model, we need to divide the data into three distinct datasets. The set of data used to train the model is called training data. The set of data used to validate the performance of the model during training is called validation data. Test data is the set of data for checking the performance of the model after completing the training. The division of these three sets is important in building a model with high generalization performance. As training data for DL, we utilized 21 figurative line-type geoglyphs discovered before 2018 (No.1-21 in Table 1). These are the

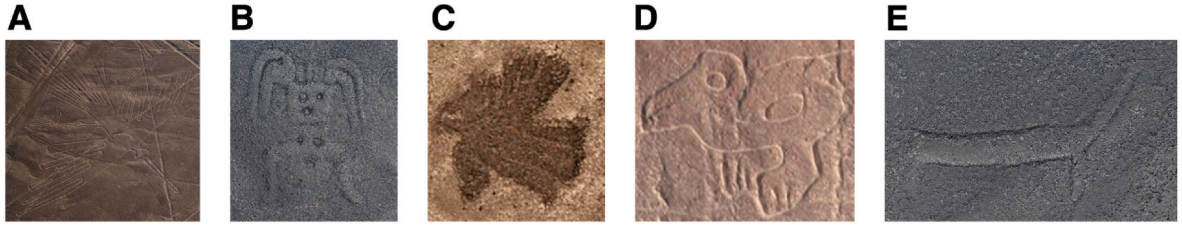

Fig. 1. Types of figurative geoglyphs. There are two main types of figurative geoglyphs: line-type and relief-type. Both were created on the Nasca Pampa covered with black stones on top of a white layer of sand. (A) "Line-type figurative geoglyphs" were made by removing black stones in a linear pattern exposing the white sand underneath. (B to E) "Relief-type figurative geoglyphs" are often located on slopes and comprise a combination of black stone and white sand surfaces. This type of geoglyph can be categorized into subtypes 1–4 as follows: (B) "Relief-type 1" was made by removing black stones to expose the white sand at the motif. Some of the removed stones were reused to depict the details of the motif. (C) "Relief-type 2" was made by removing black stones around the motif. Some of the removed stones were piled on top of the motif to make it more prominent. (D) "Relief-type 3" was made by removing black stones along the outline of the motif and by piling the removed stones on top of the motif. (E) "Relief-type 4" is white because it was made by removing all the black stones from the inside of the motif.

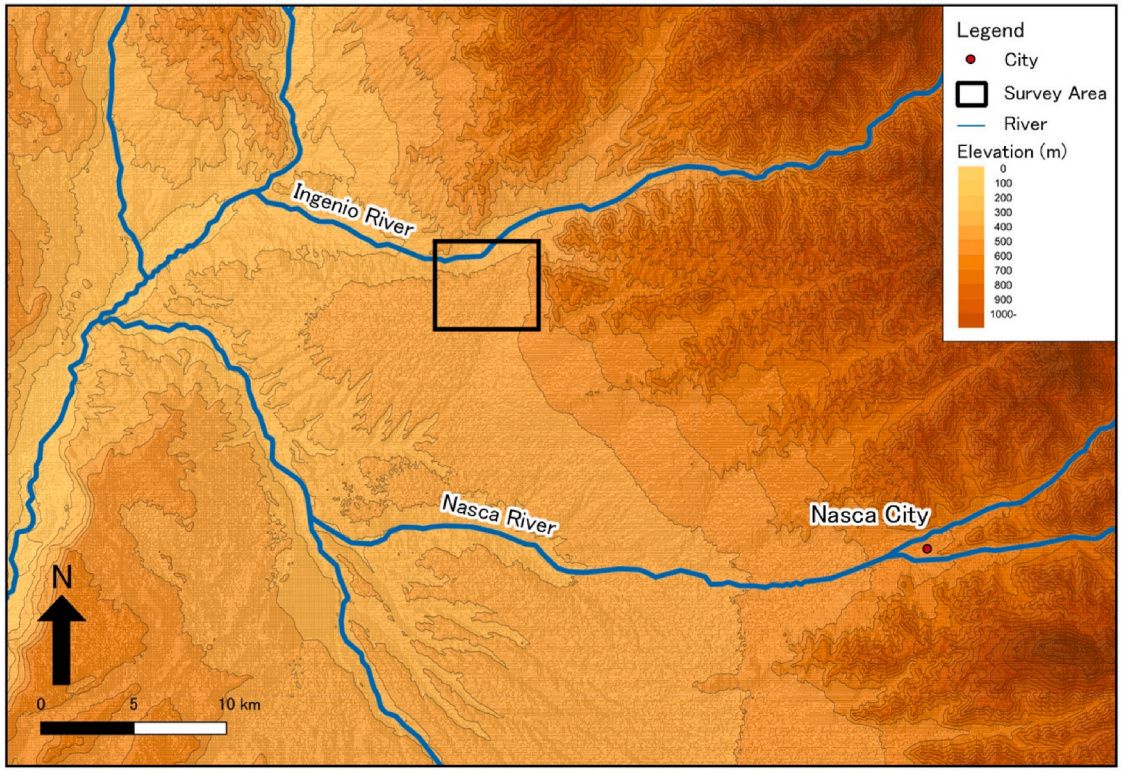

Fig. 2. Survey area in this study. Northern area of the Nasca Pampa, the area enclosed by the square is the survey area (Latitude 14°40′11″–14°42′47″S and longitude 75°5′44″–75°8′52″W).

geoglyphs representing animals drawn in the flat areas of the Nasca Pampa. Most of these geoglyphs exceed 50 m. We used four geoglyphs of the same type as validation data (Val data) for DL (No.22-25 in Table 1). As a separate set of test data evaluating training performance, we used seven figurative line-type geoglyphs discovered before 2018 (No.26-32 in Table 1). The dataset was selected by archaeologists. The training data were selected from well-known ground geoglyphs, while the test data were selected from lesser-known ones. To avoid arbitrariness in DL model creation due to prior knowledge of test data, the test data was shared with the DL model developer working on the PoC after the DL model was created.

2.2. Approach for training data

To identify new geoglyph's candidates in aerial photographs, we developed an object detection pipeline based on DL. We investigated strategies to handle the following specific issues unique to archaeology:

i. The design of each geoglyph is unique. We assumed that new geoglyphs do not have the same design as the existing ones. DL is not suited for finding features that do not exist in the training data selected from the known geoglyphs. Therefore, finding new geoglyphs is a hard task for DL.
ii. The amount of training data is small. Twenty-one geoglyphs were at hand for training DL algorithms. However, typical DL object detection models are trained using datasets with thousands to millions of annotated objects (Mogelmose et al., 2012; Lin et al., 2014).
iii. Figurative line-type geoglyphs have a variety of sizes, which range from less than 10 m to more than 300 m.

We developed an approach to labeling training data. Labeling is the process of surrounding the entire object to capture by a rectangle frame termed a "Bounding Box (BBox)" (He et al., 2019) with a certain class name attribute. To resolve issue (i) and (ii), we implemented labeling to detect new geoglyphs based on similarities in certain parts rather than the entire geoglyph. We assumed that there is a similar partial pattern between the known and new geoglyphs. By simplifying the pattern in the BBox, we aimed to detect even a small part of a new geoglyph. Specifically, we defined a unit called "element" as a class name. The "element" is a part of a geoglyph that has the minimum necessary features needed to recognize an area enclosed by BBox as a geoglyph. For example, we labeled parts such as the heads, torsos, arms, legs, and tails as "elements" for animal geoglyphs (Fig. 3A). Since the BBox is rectangular, other parts may be included when the BBox area is large. In such cases, further division into smaller elements eliminates other parts. For example, an arm can be divided into the upper arm, forearm, hand, etc. (Fig. 3B). Such division excludes any other geoglyphs from the BBox. In addition, we could increase the amount of training data by defining the "element". As a result of labeling geoglyphs based on the "element" guideline, the 21 geoglyphs became 95 "elements" with independent shapes. We used these elements as training data for object detection (Fig. 4B)..

For training, we used a COCO dataset (Lin et al., 2014) pretrained model as initial model to achieve better accuracy and reduce training time (Fig. 4D)..

Regarding issue (iii), by cropping the original images in multiscale,

Table 1
Information on newly discovered geoglyphs and geoglyphs used in PoC.

No.	Training data	Val data	Test data	New geoglyph	Design	Type	Size (meter)	Figure
1	✓				Geometric	line-type	31	
2	✓				Killer Whale	line-type	28	
3	✓				Legs	line-type	51	
4	✓				Plant	line-type	49	
5	✓				Bird	line-type	60	
6	✓				Spider	line-type	47	
7	✓				Fox	line-type	50	
8	✓				Fish	line-type	65	
9	✓				Geometric	line-type	79	
10	✓				Bird	line-type	216	
11	✓				Plant	line-type	85	
12	✓				Delta	line-type	116	
13	✓				Bird	line-type	98	
14	✓				Bird	line-type	110	
15	✓				Lizard	line-type	188	
16	✓				Fan	line-type	127	
17	✓				Monkey	line-type	94	
18	✓				Bird	line-type	218	
19	✓				Bird	line-type	237	
20	✓				Bird	line-type	303	
21	✓				Bird	line-type	382	
22		✓			Pin	line-type	46	
23		✓			Plant	line-type	53	
24		✓			Bird	line-type	52	
25		✓			Bird	line-type	129	
26			✓		Animal	line-type	16	Fig. 5G
27			✓		Bird	line-type	9	Fig. 5E
28			✓		Geometric	line-type	37	Fig. 5F
29			✓		Fish	line-type	30	Fig. 5C
30			✓		Killer Whale	line-type	41	Fig. 5D
31			✓		Pin	line-type	43	Fig. 5B
32			✓		Animal	line-type	87	Fig. 5H
33				✓	Humanoid	relief-type	5	Fig. 6A
34				✓	Fish	relief-type	19	Fig. 6C
35				✓	Bird	line-type	17	Fig. 6D
36				✓	Pair of legs	line-type	78	Fig. 6B

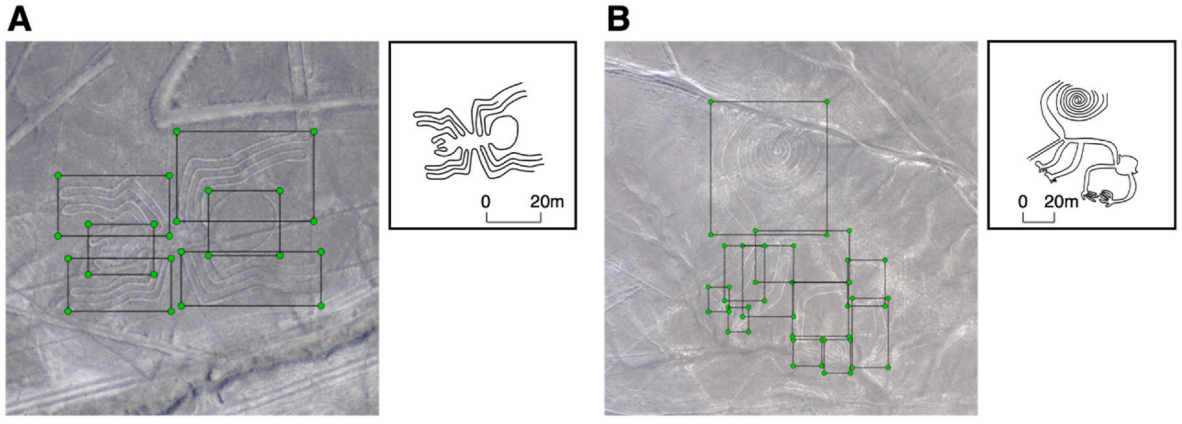

Fig. 3. Examples of BBox labeling based on "element" rules. (**A**) For spider geoglyphs, the head, legs, and body are each counted as one element. (**B**) For the legs and arms of monkey geoglyphs, the arm and area beyond the wrist and the leg and the area beyond the ankle are counted as separate elements.

many variations of input images with different ratios between the cropped image width and geoglyph width were generated for the same geoglyph (and element). With this technique, we supported the detection of geoglyphs of varying sizes (Fig. 4C).

2.3. Policy for detection threshold

We adjusted the number of candidates to be detected by changing a confidence score threshold for object detection (Fig. 4F). In object detection, individual detection results are a BBox around the identified object with its confidence score. In general, the threshold is set high enough to limit over-detection. In this study, we controlled the threshold intentionally to get a certain number of candidates. In other words, we want to avoid overlooking True Positive at the expense of a relatively large number of False Positive. True Positive refers to geoglyphs that the DL model detected correctly, while False Positive refers to geoglyphs that the DL model detected with BBox incorrectly.

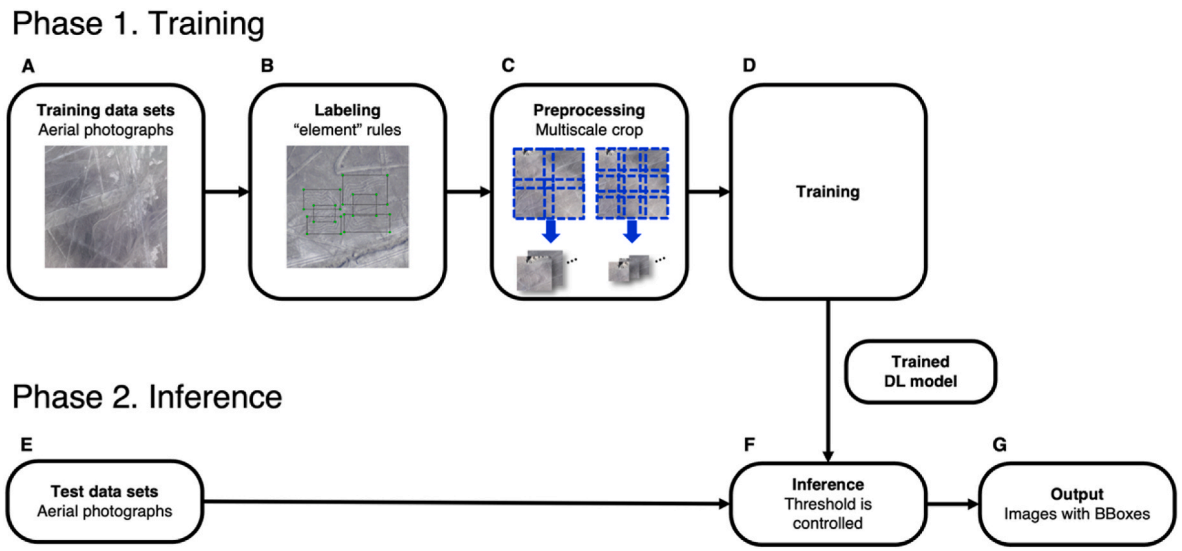

Fig. 4. Unified pipeline for Nasca geoglyphs detection from aerial photographs in training and inference phase. (**A**) Aerial photographs that contain Nasca geoglyphs as training data. (**B**) Labeling of geoglyphs based on "element" rules. (**C**) Cropping aerial photographs to various sizes. (**D**) Training with cropped images as input for DL. (**E**) Aerial photographs that contain Nasca geoglyphs as test data. (**F**) Applying object detection using the trained DL model. (**G**) The output are images with the BBoxes which are candidates of geoglyphs.

3. Results

3.1. Results of detecting test data

We made inference with the trained DL model of object detection against aerial photographs and output candidates of geoglyphs. With a confidence score threshold of 0.9, 1954 "elements" were detected (Fig. 5A). While checking against the seven test geoglyphs, the model detected five of them (Fig. 5B–F). In contrast, when we initially labeled one entire geoglyph with one BBox instead of the "element" approach, the model could not detect any test geoglyph. Therefore, this result indicates that defining and training DL model using "element" as labels is effective for detecting geoglyphs.

The five detected geoglyphs were a bird, orca, fish, hand, and pin ranging in length from 10 to 70 m. Among these, three were distributed in the flat area of the Nasca Pampa (Fig. 5B–D). The remaining two were distributed in the Ventilla (Ingenio Valley) of the sloped portion of the northern area of the Nasca Pampa (Fig. 5E and F). A common feature of the five geoglyphs is that they exist in a similar sandy ground surface as that of the training data and the lines stuck out from the surrounding ground surface.

Two test geoglyphs could not be detected. One is a 16-m-long line-type estimated to be animal, created in the flat part of the Nasca Pampa (Fig. 5G). The region where it was drawn has a whitish ground surface due to the liquid flowing through it in the past. Thus, even if the pebbles on the ground surface for the geoglyph were removed, the geoglyph was extremely unlikely to be visible because there was very little difference in the color of the ground surface and exposed surface. The other one is an 87-m-long line-type animal created in the sloped part of the north edge of the Nasca Pampa (Fig. 5H), called the San Miguel de la Pascana region. It is less visible than the geoglyphs drawn in the flat areas. The geoglyphs drawn in this area are not included in the training data. Moreover, the training and test data was chosen by the archaeologist and the test data was not shared in advance, the DL developer could not take these reginal conditions into account when creating the DL model. Therefore, the DL model may not be able to learn the ground surface features of this area.

In the Nasca Pampa, there are several geometric patterns, such as straight-line geoglyphs, modern roads, and ruts. We do not intend to detect these targets. Because the amount of training data is limited, the trained model exhibits little discriminative capacity to separate geoglyphs from such types of ambiguous patterns. Therefore, geometric patterns other than the targets were over-detected (Fig. 5, I to L).

3.2. Detection against new geoglyph's candidates

It is encouraging that the trained models detected five of seven geoglyphs of test data. Therefore, we searched for new geoglyph's candidates using this model. Consequently, we discovered four new geoglyphs. Three of them (Fig. 6B–D) were geoglyphs that are reported for the first time in this paper. When the confidence score threshold was set to 0.9, 1954 "elements" were detected. First, we selected one candidate for a new geoglyph out of these (Fig. 6A). After the on-site survey, we confirmed that it was indeed an undiscovered geoglyph. Due to this fact, further investigation was conducted on all of the 0.9 threshold detection results, and we found another candidate (Fig. 6B). Subsequently we set the threshold to 0.7. The number of "elements" has increased to 4587. We could extract two additional candidates out of the added detection results (Fig. 6C and D). These two were also confirmed to be new geoglyphs by the on-site survey.

In these newly discovered geoglyphs, a humanoid (Fig. 6A), a pair of legs (or hands) (Fig. 6B), a fish (Fig. 6C), and a bird (Fig. 6D) are drawn. Though similar designs can be found in previously discovered geoglyphs, the four new ones are quite unique. Among these, a humanoid geoglyph holding a club in his/her right hand is a mixture of subtypes 1 and 2 of relief-type with a length of 5 m. The pair-of-legs geoglyph is a line-type with a length of 78 m. The fish geoglyph with a wide-open mouth is a mixture of subtypes 2 and 3 of the relief types with a length of 19 m. The bird geoglyph is a line-type with a length of 17 m. Rather than just being a simple bird form, it is a design combining straight lines and curves to form a bird.

The relief-type is different from the line-type in the way it is made, but some relief-type geoglyphs have a line-like feature that distinguishes them from their surroundings in photographs. Therefore, the relief-type geoglyphs sometimes look like line-type. For example, the humanoid geoglyph comprises a rectangular part corresponding to a face, while the decorations on the head and club in the hand comprise multiple lines. The fish geoglyph has outline of line-like features and overlaps with lineal geoglyphs. Thus, although the two geoglyphs are relief-type, they were detected because their BBoxes have line-like features similar to

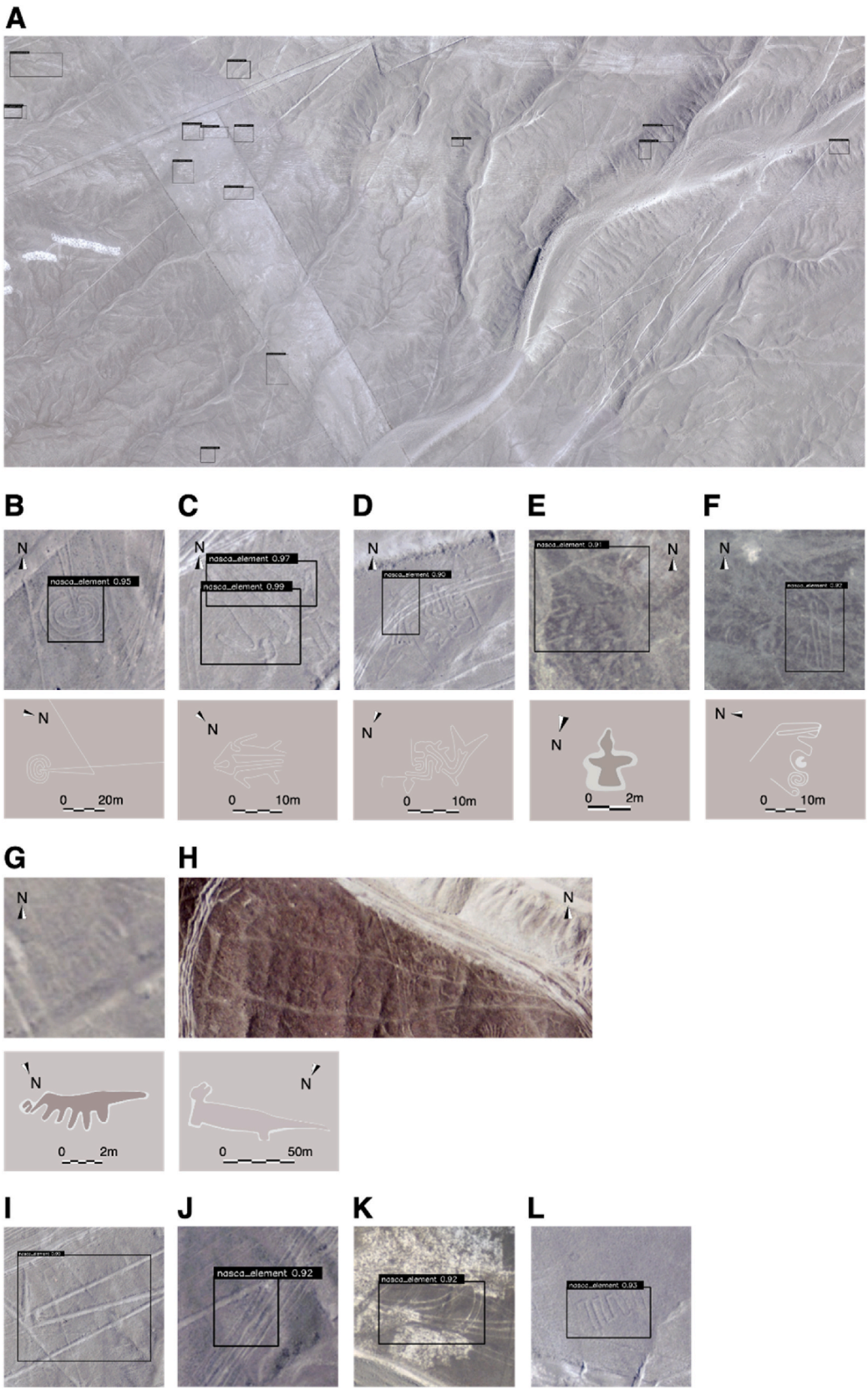

Fig. 5. Inference results of aerial photographs. (**A**) Examples of inference result of aerial photographs. This is part of aerial photographs used for testing that are within the Northern part of Nasca Pampa (400 m × 800 m). (**B** to **L**) The inference results of the DL model. (**B** to**F**) Detected test data. (**G** to **H**) Undetected test data. (**I** to **L**) Over-detected items.

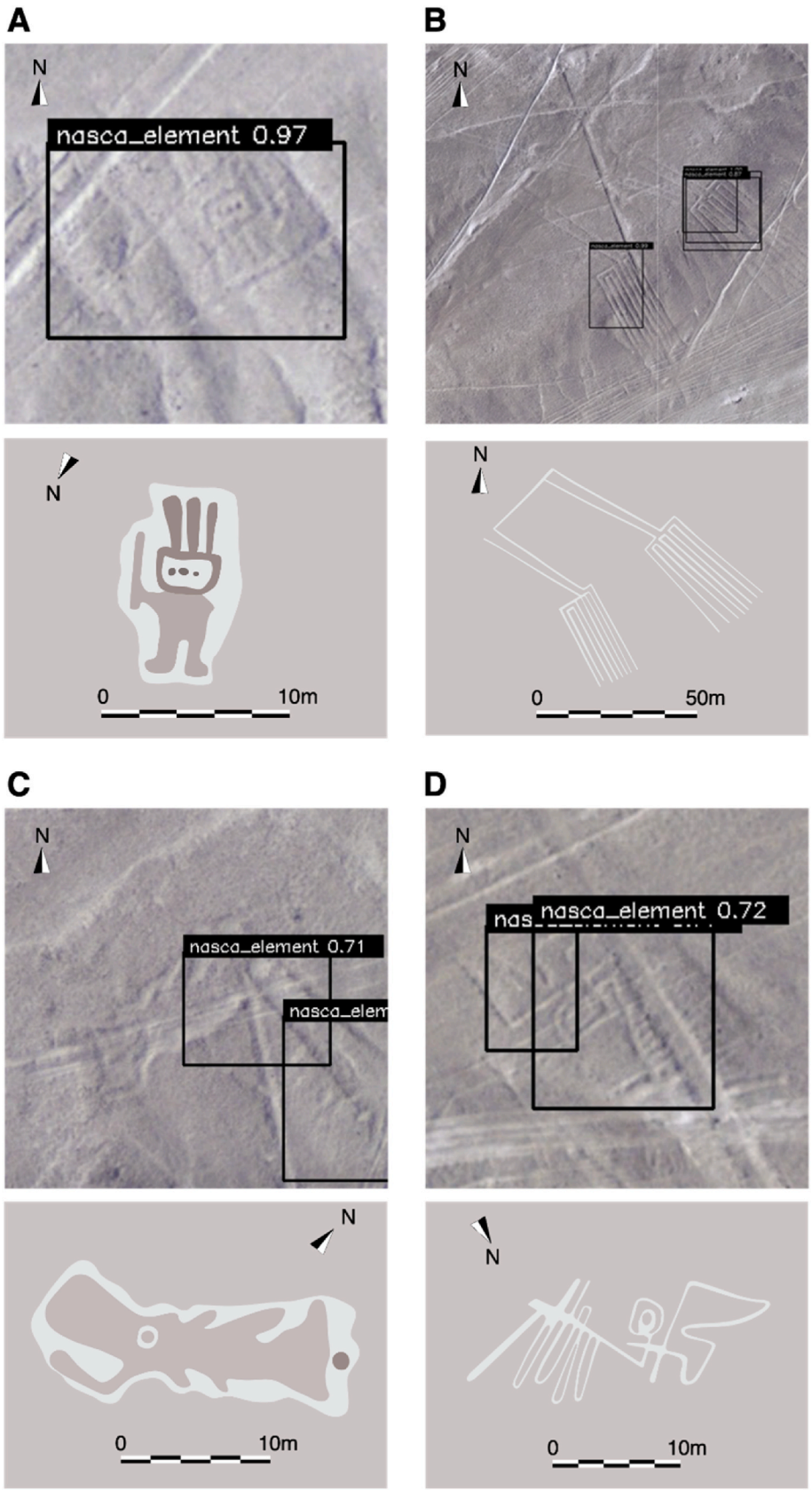

Fig. 6. Four new Nasca geoglyphs identified by Deep Learning. (**A**) A humanoid, relief-type (No.33 in Table 1). (**B**) A pair of legs, line-type (No.36 in Table 1). (**C**) A fish, relief-type (No.34 in Table 1). (**D**) A bird, line-type (No.35 in Table 1). (B to D) are presented to the public for the first time in this paper.

trained "element," thereby this result agrees well with our approach for detection.

4. Discussion

4.1. Strategies to reduce False Negatives

Two False Negatives occurred in the test data. False Negatives refer to targets that we would ideally like to detect using DL but are overlooked. In this section, we discuss the causes and possible improvements for False Negatives and highlight the significance of our proposed method.

We assume that the cause of the False Negatives is the lack of training data for the DL. In DL projects, sufficient training data is often not available initially, so the general approach is to go through several cycles of collecting data and building models to gradually improve accuracy. The model used in this study was at the PoC stage, and the main objective was an initial evaluation of the effectiveness of the method. The DL model uses only the known geoglyphs shown in Table 1 as training data. Therefore, the model did not cover a wide variety of geoglyph's patterns and ground surface features, creating a situation prone to False Negatives.

Although it is difficult to completely eliminate False Negative in DL, detection accuracy may be improved by adding training data. For example, the DL model created in this study has only learned geoglyphs from a part of the Nasca Pampa. By learning geoglyphs from other parts of the Nasca Pampa as well, the patterns of recognizable targets will increase, potentially leading to improved accuracy. It is also effective to add False Negative data as training data.

In this study, we evaluated the method of utilizing DL in geoglyph research using SSD object detection model, and clarified its effectiveness. Object detection in DL includes various algorithms other than SSD, such as one-stage detector, represented by YOLO, etc. which simultaneously performs object region extraction and category identification, and two-stage detector, represented by R–CNN etc., which performs these processes in series (Zou et al., 2023). Each of these algorithms has different characteristics of image processing, inference speed, and accuracy. In recent years, there have been efforts to apply Transformers, used in generative AI, to object detection (Han et al., 2023). Therefore, in addition to enhancing training data, the following approaches are also considered effective for further improvement of accuracy.

- Evaluation and comparison of each algorithm in terms of usefulness and improvement of accuracy in detecting geoglyphs.
- Investigation of an ensemble method (Ganaie et al., 2022) that uses multiple algorithms and compensates for differences in their characteristics to improve overall accuracy.

We believe that these improvement ideas will reduce not only False Negatives but also False Positives caused by similar factors. In other words, we can minimize overlooking targets while suppressing the rate of false detections, leading to more accurate output.

4.2. Significance of the proposed method

The significance of our method is that DL can be used as a support tool for researchers. Even with human visual inspection, there are cases of missed or unrecognized geoglyphs. For example, the newly discovered human geoglyph (Fig. 6A) was near the famous hummingbird geoglyph but had never been found before. With the aid of DL, more geoglyphs can be discovered. Although DL cannot guarantee 100% detection, its accuracy can be improved by adding training data, and in some cases it exceeds human accuracy. In addition, for issues (ii) and (iii) peculiar to geoglyphs, the accuracy is improved by utilizing the elements and multiscale crops proposed in this paper. By enhancing accuracy, the level of assistance is increased, and more geoglyphs can be expected to be discovered.

Furthermore, geoglyphs currently face the risk of destruction, and it is imperative to identify and protect as many geoglyphs as possible. Improvements in photography technology have made it possible to discover small geoglyphs that could not be found before, but the amount of image data to be investigated is enormous. Checking all these images manually requires a significant amount of effort. DL can process large amounts of data as long as computing resources are available, thus accelerating the investigation. The specific measurement of its effectiveness is discussed in the next section. In this way, the proposed method is expected to contribute to the discovery and protection of geoglyphs.

4.3. Acceleration of research

Using this DL approach, we were able to significantly reduce the time required to investigate the distribution of new geoglyphs. It took us five years to identify and map not only figurative geoglyphs, but also lineal and geometric ones from satellite images of the entire Nasca Pampa. The ground resolution of these satellite images is 0.61 m per pixel. On the other hand, in this study we used high-resolution aerial photographs with a ground resolution of 0.1 m per pixel. Therefore, a much longer time was expected to be required to perform the same work compared to using satellite images. By introducing the DL model, we were able to drastically reduce this work time and effectively used the high-resolution aerial photographs for geoglyph detection. Specifically, the DL approach is calculated to make the task of examining aerial photographs approximately 21 times faster. We estimated the time required for an experienced and knowledgeable archaeologist to visually identify the geoglyphs. The aerial photograph of the target area comprised 42 high-resolution images, covering about 9% of the total Nasca Pampa area. It took 3.5 h for the archaeologist to identify only figurative geoglyphs in one image using his/her eyes. If the same task was done for the entire Nasca Pampa, it would require about 1633 h according to the calculation. However, we estimate that using the DL model for the Nasca Pampa it will take only about 78 h for the archaeologist to visually verify the geoglyph candidates detected. This is because the DL approach simplifies this task for the archaeologist as a work of classifying the detected BBox into True Positive and False Positive. This means that the introduction of DL has greatly reduced the time and effort of archaeologists.

4.4. Extension to relief-type

For further advanced research of figurative geoglyphs, new "elements" for recognizing relief-type geoglyphs are also need to be defined. The relief-type geoglyphs have four subtypes according to the different methods by which they were created (Fig. 1), and they vary in appearance depending on the soil texture of the ground on which they are depicted. It is important to investigate how these differences are reflected in the features of the image data. Many relief-type geoglyphs are located on slopes, therefore aerial photographs taken from above are not always useful for detecting geoglyphs. Integrating the image data of geoglyphs with topographic data acquired using LiDAR is expected to increase the detection rate of the relief-type geoglyphs. The DL model trained with line-type geoglyphs allowed us to discover two relief-type geoglyphs. The reason for determining the relief-type geoglyphs is that the lines and curves in the relief-type were recognized as the "element" of the line-type in DL. This confirms that the DL analysis does not necessarily correspond to the classification of geoglyphs by archaeologists and indicates the possibility of further archaeological classification of relief-type geoglyphs.

4.5. Conclusions

We have developed a DL pipeline that addresses the challenges that

commonly arise in the task of archaeological image object detection. Our approach allows DL to learn representations of images with better generalization performance, enabling the discovery of targets that have been difficult to find in the past. Moreover, by accelerating the research process, our method contributes to archaeology by establishing a new paradigm that combines field surveys and AI, leading to more efficient and effective investigations.

Author contributions

Conceptualization: MS, YL, MH, KN; Formal Analysis: YL, MH; Funding acquisition: MS; Investigation: MS, JO; Methodology: MS, YL, MH, KN; Project administration: MS, TL, MH; Resources: MS, YL, JO, MH, KN: Software: KN; Supervision: MS; Visualization: MS, YL, JO; Writing – original draft: MS, YL, MH, KN; Writing – review & editing: MS, YL, JO, MH, KN.

Funding

This study was supported by research grants from Japan Society for the Promotion of Science KAKENHI (grant no. 20H00041) and by Yamagata University YU-COE(S)(S-4).

Declaration of competing interest

The authors declare that they have no known competing financial interests or personal relationships that could have appeared to influence the work reported in this paper.

Acknowledgments

This study arises from a collaboration between Yamagata University and IBM Japan. We thank Masato Abukawa, Taketoshi Miyama for the coordination; Akihisa Sakurai, Hendrik Hamann, Siyuan Lu, Marcus Freitag, Conrad Albrecht, Muneki Yasuda, Atsushi Tanaka, Kevin Vaughn, Kaoru Honda for helpful suggestions; Yoshimitsu Ccoyllo, Yuichi Matsumoto, Atsushi Yamamoto, Yuko Ito for geoglyph research.

Appendix A. Supplementary data

Supplementary data to this article can be found online at https://doi.org/10.1016/j.jas.2023.105777.

References

Albrecht, C.M., Fisher, C., Freitag, M., Hamann, H.F., Pankanti, S., Pezzutti, F., Rossi, F., 2019. Learning and recognizing archeological features from LiDAR data. In: 2019 IEEE International Conference on Big Data (Big Data). Presented at the 2019 IEEE International Conference on Big Data (Big Data), pp. 5630–5636. https://doi.org/10.1109/BigData47090.2019.9005548.

Aveni, A.F. (Ed.), 1990. The Lines of Nazca. American Philosophical Society, Philadelphia.

Barucci, A., Canfailla, C., Cucci, C., Forasassi, M., Franci, M., Guarducci, G., Guidi, T., Loschiavo, M., Picollo, M., Pini, R., Python, L., Valentini, S., Argenti, F., 2022. Ancient Egyptian hieroglyphs segmentation and classification with convolutional neural networks. In: Furferi, R., Governi, L., Volpe, Y., Seymour, K., Pelagotti, A., Gherardini, F. (Eds.), The Future of Heritage Science and Technologies: ICT and Digital Heritage, Communications in Computer and Information Science. Springer International Publishing, Cham, pp. 126–139. https://doi.org/10.1007/978-3-031-20302-2_10.

Barucci, A., Cucci, C., Franci, M., Loschiavo, M., Argenti, F., 2021. A deep learning approach to ancient Egyptian hieroglyphs classification. IEEE Access 9, 123438–123447. https://doi.org/10.1109/ACCESS.2021.3110082.

Bonhage, A., Eltaher, M., Raab, T., Breuß, M., Raab, A., Schneider, A., 2021. A modified Mask region-based convolutional neural network approach for the automated detection of archaeological sites on high-resolution light detection and ranging-derived digital elevation models in the North German Lowland. Archaeol. Prospect. 28, 177–186. https://doi.org/10.1002/arp.1806.

Caspari, G., Crespo, P., 2019. Convolutional neural networks for archaeological site detection -Finding "princely" tombs. J. Archaeol. Sci. 110 https://doi.org/10.1016/j.jas.2019.104998.

Character, L., Ortiz JR., A., Beach, T., Luzzadder-Beach, S., 2021. Archaeologic machine learning for shipwreck detection using lidar and sonar. Rem. Sens. 13, 1759. https://doi.org/10.3390/rs13091759.

Clanuwat, T., Lamb, A., Kitamoto, A., 2019. KuroNet: Pre-modern Japanese Kuzushiji Character Recognition with Deep Learning. https://doi.org/10.48550/arXiv.1910.09433.

Clarkson, P.B., 1990. The archaeology of the Nazca pampa: environmental and cultural parameters. In: Aveni, Anthony F. (Ed.), The Lines of Nazca. American Philosophical Society, pp. 115–172.

Davis, D.S., Caspari, G., Lipo, C.P., Sanger, M.C., 2021. Deep learning reveals extent of Archaic Native American shell-ring building practices. J. Archaeol. Sci. 132, 105433 https://doi.org/10.1016/j.jas.2021.105433.

Ganaie, M.A., Hu, M., Malik, A.K., Tanveer, M., Suganthan, P.N., 2022. Ensemble deep learning: a review. Eng. Appl. Artif. Intell. 115, 105151 https://doi.org/10.1016/j.engappai.2022.105151.

Goodfellow, I., Bengio, Y., Courville, A., 2016. Deep Learning. The MIT Press, Cambridge, Massachusetts.

Guyot, A., Lennon, M., Hubert-Moy, L., 2021a. Objective comparison of relief visualization techniques with deep CNN for archaeology. J. Archaeol. Sci. Rep. 38, 103027 https://doi.org/10.1016/j.jasrep.2021.103027.

Guyot, A., Lennon, M., Lorho, T., Hubert-Moy, L., 2021b. Combined detection and segmentation of archeological structures from LiDAR data using a deep learning approach. J. Comput. Anal. Appl. 4, 1–19. https://doi.org/10.5334/jcaa.64.

Han, K., Wang, Y., Chen, H., Chen, X., Guo, J., Liu, Z., Tang, Y., Xiao, A., Xu, C., Xu, Y., Yang, Z., Zhang, Y., Tao, D., 2023. A survey on vision transformer. IEEE Trans. Pattern Anal. Mach. Intell. 45, 87–110. https://doi.org/10.1109/TPAMI.2022.3152247.

He, Y., Zhu, C., Wang, J., Savvides, M., Zhang, X., 2019. Bounding Box regression with uncertainty for accurate object detection. In: Proceedings of the IEEE/CVF Conference on Computer Vision and Pattern Recognition (CVPR). https://doi.org/10.48550/arXiv.1809.08545. Presented at the CVPR 2019, arXiv.

Isbell, W.H., 1978. The prehistoric ground drawings of Peru. Sci. Am. 239 (4), 140–153.

Kazimi, B., Thiemann, F., Malek, K., Sester, M., Khoshelham, K., 2018. Deep learning for archaeological object detection in airborne laser scanning data. In: Proceedings of the 2nd Workshop on Computing Techniques for Spatio-Temporal Data in Archaeology and Cultural Heritage, pp. 22–28. Melbourne, Australia.

Kosok, P., 1965. Life, Land, and Water in Ancient Peru. Long Island University Press, Brooklyn.

Kroeber, A.L., Collier, D., 1998. The Archaeology and Pottery of Nazca, Peru: Alfred L. Kroeber's 1926 Expedition. AltaMira Press, Walnut Creek.

Lamb, A., Clanuwat, T., Kitamoto, A., 2020. KuroNet: regularized residual U-nets for end-to-end kuzushiji character recognition. SN Comput. Sci. 1, 177. https://doi.org/10.1007/s42979-020-00186-z.

Lambers, K., 2020. Walking and marking the desert: geoglyphs in arid South America. In: A Human Environment. Studies in Honour of 20 Years Analecta Editorship by Prof. Dr. Corrie Bakels (Analecta Praehistorica Leidensia 50). Sidestone Press, pp. 89–106.

Lambers, K., 2006. The geoglyphs of Palpa, Peru: Documentation, analysis, and interpretation, Forschungen zur Archäologie Außereuropäischer Kulturen 2. Aichwald.

Lidar 101: An Introduction to Lidar Technology, 2012. Digit. Coast Train. URL Data, and Applications [WWW Document]. accessed 10.21.22. https://coast.noaa.gov/digitalcoast/training/lidar-101.html.

Lin, T.-Y., Maire, M., Belongie, S., Hays, J., Perona, P., Ramanan, D., Dollár, P., Zitnick, C.L., 2014. Microsoft COCO: common objects in context. In: Fleet, D., Pajdla, T., Schiele, B., Tuytelaars, T. (Eds.), Computer Vision – ECCV 2014, Lecture Notes in Computer Science. Springer International Publishing, Cham, pp. 740–755. https://doi.org/10.1007/978-3-319-10602-1_48.

Liu, L., Ouyang, W., Wang, X., Fieguth, P., Chen, J., Liu, X., Pietikäinen, M., 2020. Deep learning for generic object detection: a survey. Int. J. Comput. Vis. 128, 261–318. https://doi.org/10.1007/s11263-019-01247-4.

Liu, W., Anguelov, D., Erhan, D., Szegedy, C., Reed, S., Fu, C.-Y., Berg, A.C., 2016. SSD: single Shot MultiBox detector. In: Leibe, B., Matas, J., Sebe, N., Welling, M. (Eds.), Computer Vision – ECCV 2016, Lecture Notes in Computer Science. Springer International Publishing, Cham, pp. 21–37. https://doi.org/10.1007/978-3-319-46448-0_2.

Lumbreras, L.G., 2000. Formulación de los lineamientos para la elaboración de un Plan de manejo de las líneas de Nasca 1: contexto arqueológico. INC, UNESCO, Lima.

Mantovan, L., Nanni, L., 2020. The computerization of archaeology: survey on AI techniques. SN Comput. Sci. 1, 267. https://doi.org/10.1007/s42979-020-00286-w.

Mejía Xesspe, T., 1942. Acueductos y caminos antiguos de la hoya del Río Grande de Nasca. Actas y trabajos científicos del XXVII Congreso Internacional de Americanistas (Lima, 1939). Librería e Imprenta Gil, Lima, pp. 559–569.

Mogelmose, A., Trivedi, M.M., Moeslund, T.B., 2012. Vision-based traffic sign detection and analysis for intelligent driver assistance systems: perspectives and survey. IEEE Trans. Intell. Transport. Syst. 13, 1484–1497. https://doi.org/10.1109/TITS.2012.2209421.

Pecci, A., 2020. Digital survey from drone in archaeology: potentiality, limits, territorial archaeological context and variables. IOP Conf. Ser. Mater. Sci. Eng. 949, 012075 https://doi.org/10.1088/1757-899X/949/1/012075.

Reiche, M., 1993. Contribuciones a la geometría y astronomía en el antiguo Perú. Asociación María Reiche para las líneas de Nasca, Lima.

Reindel, M., Isla, J., Koschmieder, K., 1999. Vorspanische Siedlungen und Bodenzeichnungen in Palpa, Südperu/Asentamientos prehispánicos y geoglifos en Palpa, costa sur del Perú. Beiträge zur Allgemeinen und Vergleichenden Archäologie 19, 313–381.

Reindel, M., Isla, J., Lambers, K., 2006. Altares en el desierto : las estructuras de piedra sobre los geoglifos Nasca en Palpa. Arqueología y Sociedad. 17, 179–222.
Roman-Rangel, E., Marchand-Maillet, S., 2016. Indexing mayan hieroglyphs with neural codes, in: 2016 23rd international conference on pattern recognition (ICPR). In: Presented at the 2016 23rd International Conference on Pattern Recognition (ICPR), pp. 253–258. https://doi.org/10.1109/ICPR.2016.7899642.
Sakai, M., Olano, J., 2017. Líneas y figuras de la Pampa de Nazca/lines and figures of the pampa de Nazca. In: Pardo, C., Fux, P. (Eds.), Nasca. Asociación Museo de Arte de Lima, Lima, pp. 124–131, 366-368.
Sakai, M., Olano, J., Matsumoto, Y., Takahashi, H., 2014. Centros de líneas y cerámica en las pampas de Nasca, Perú, 2010. Yamagata University Press, Yamagata.
Sakai, M., Olano, J., Takahashi, H., 2021. Líneas y Cerámica en las Pampas de Nasca, Perú, 2011-2013. Yamagata University Press, Yamagata.
Sakai, M., Olano, J., Takahashi, H., 2019. Centros de Líneas y Cerámicas en las Pampas de Nasca, Perú, hasta el año 2018. Yamagata University Press, Yamagata.
Soroush, M., Mehrtash, A., Khazraee, Ur J., 2020. Deep learning in archaeological remote sensing: automated qanat detection in the kurdistan region of Iraq. Rem. Sens. 12, 500. https://doi.org/10.3390/rs12030500.
Specia, M., 2018. 'Deep Scars' as Trucker Drives across Peru's 2,000-Year-Old Nazca Lines. N. Y. Times.
Trier, Ø.D., Reksten, J.H., Løseth, K., 2021. Automated mapping of cultural heritage in Norway from airborne lidar data using faster R-CNN. Int. J. Appl. Earth Obs. Geoinformation 95, 102241. https://doi.org/10.1016/j.jag.2020.102241.
Vaart, W.B.V. der, Lambers, K., 2019. Learning to look at LiDAR: the use of R-CNN in the automated detection of archaeological objects in LiDAR data from The Netherlands. J. Comput. Anal. Appl. 2, 31–40. https://doi.org/10.5334/jcaa.32.
Zhu, X.X., Tuia, D., Mou, L., Xia, G.-S., Zhang, L., Xu, F., Fraundorfer, F., 2017. Deep learning in remote sensing: a comprehensive review and list of resources. IEEE Geosci. Remote Sens. Mag. 5, 8–36. https://doi.org/10.1109/MGRS.2017.2762307.
Zou, Z., Chen, K., Shi, Z., Guo, Y., Ye, J., 2023. Object detection in 20 Years: a survey. Proc. IEEE 111, 257–276. https://doi.org/10.48550/arXiv.1905.05055.